MICROBIOME

Microbiome-derived inosine modulates response to checkpoint inhibitor immunotherapy

Lukas F. Mager[1]*, Regula Burkhard[2], Nicola Pett[1], Noah C. A. Cooke[1], Kirsty Brown[1], Hena Ramay[3], Seungil Paik[4], John Stagg[5], Ryan A. Groves[6], Marco Gallo[4], Ian A. Lewis[6], Markus B. Geuking[2], Kathy D. McCoy[1]*

Several species of intestinal bacteria have been associated with enhanced efficacy of checkpoint blockade immunotherapy, but the underlying mechanisms by which the microbiome enhances antitumor immunity are unclear. In this study, we isolated three bacterial species—*Bifidobacterium pseudolongum*, *Lactobacillus johnsonii*, and *Olsenella* species—that significantly enhanced efficacy of immune checkpoint inhibitors in four mouse models of cancer. We found that intestinal *B. pseudolongum* modulated enhanced immunotherapy response through production of the metabolite inosine. Decreased gut barrier function induced by immunotherapy increased systemic translocation of inosine and activated antitumor T cells. The effect of inosine was dependent on T cell expression of the adenosine A_{2A} receptor and required costimulation. Collectively, our study identifies a previously unknown microbial metabolite immune pathway activated by immunotherapy that may be exploited to develop microbial-based adjuvant therapies.

Immune checkpoint blockade (ICB) therapy can be an effective therapy in some tumors and certain cancer patients by harnessing the therapeutic potential of the immune system. Targeting cytotoxic T lymphocyte–associated antigen 4 (CTLA-4) or programmed cell death protein 1 (PD-1) or its ligand (PD-L1) has revolutionized the treatment of some cancers, including melanoma, renal cell carcinoma, and non–small cell lung cancer (1, 2). Nevertheless, many other cancers show primary resistance to ICB therapy, and response rates remain low and differ between patients, even in those cancers where ICB therapy has provided benefit (3–5). There is therefore an urgent need to determine the underlying reasons for such nonresponsiveness. Recent studies have provided strong evidence that the gut microbiota can affect antitumor immunity, and composition of the intestinal microbiome may even predict the efficacy of ICB therapy. A series of seminal studies revealed that the efficacy of ICB therapies was dependent on specific gut bacteria (6–10) and that treatment with ICB-promoting bacteria

may help overcome primary resistance to ICB therapies (8). Despite the findings that specific bacterial species have been associated with increased antitumor immunity, the precise molecular mechanisms by which these microbes enhance ICB therapy remain elusive. In this study, we used an animal model of colorectal cancer (CRC) to identify specific ICB-promoting bacteria, elucidated the underlying molecular mechanism of how these microbes enhanced ICB therapy efficacy, and validated our findings in additional models of bladder cancer and melanoma.

Although the intestinal microbiota can affect CRC progression (11, 12) and may alter the efficacy of chemotherapeutics (13, 14), clinically, ICB therapies are notoriously ineffective in most CRC cases (15), and the role of the microbiome in nonresponsiveness has not yet been determined. We therefore investigated the efficacy of ICB therapy in a mouse model where colonic tumors are induced using azoxymethane (AOM) and dextran sulfate sodium (DSS) (Fig. 1A). Treatment with anti-CTLA-4 or anti-PD-L1 antibodies led to significantly fewer and smaller tumors (Fig. 1, B and C) and reduced the frequency of EpCam+ Lgr5+ cells in the tumor, which are markers for epithelial cell stemness (Fig. 1D). Anti-CTLA-4 treatment also resulted in increased immune cell infiltration into the tumors (Fig. 1E). Increased CD8+ T cell frequencies in the tumor-draining lymph node (fig. S1A) was also observed together with increased IFN-γ+CD4+ and IFN-γ+CD8+ T cells in the spleen (IFN-γ, interferon-γ) (fig. S1, B and C). In this model, the effects of anti-CTLA-4 were greater than those induced by anti-PD-L1 treatment when using the same antibody dose. The difference in anti-CTLA-4 and anti-PD-L1 efficacy in this model may be dependent on the dose-

effect relationship, and higher doses have previously been described for anti-PD-1 therapy (8). Moreover, effector functions of anti-CTLA-4 and anti-PD-1 or anti-PD-L1 rely on distinct mechanisms, among them regulatory T cells (T_{regs}) (16), and indeed T_{reg} composition and function are different between cancer types (17). We next used this model system to screen for potentially beneficial bacteria that were associated with ICB responsiveness. Although no significant changes were observed in the overall fecal bacterial composition (β-diversity) between ICB-treated and control mice (fig. S1D), a few bacterial families were differentially abundant (fig. S1E). In contrast, sequencing of tumor-associated bacterial communities revealed differences in β-diversity (fig. S1F), and additional bacterial genera were differentially abundant in the ICB-treated tumors (Fig. 1F and fig. S1, G and H). We therefore performed anaerobic culture of homogenized tumors from both groups and were able to culture and identify 21 distinct bacterial isolates. Seven bacterial species were cultured only from ICB-treated tumors, whereas four were found only in the control group (Fig. 1G). *Bifidobacterium pseudolongum* was one of the isolates cultured only from ICB-treated tumors. *B. pseudolongum* belongs to the genus *Bifidobacterium*, which was identified as differentially abundant by sequencing (Fig. 1F and fig. S1, G and H). Interestingly, *Akkermansia muciniphila*, which was recently identified to enhance the efficacy of anti-PD-L1 and anti-PD-1 treatments in lung and kidney cancers (8), was also one of the seven bacteria cultured only from ICB-treated tumors (Fig. 1G). Isolation and identification of distinct bacterial species associated with ICB responsiveness provided us with the opportunity to identify the molecular mechanism involved.

Next, we determined whether the efficacy of ICB therapy in CRC was dependent on the microbiota, as has been shown with other tumor types (6). As the development of orthotopic adenocarcinomas is severely reduced in animals with a limited microbiota (18), we switched to a heterotopic in vivo model of CRC where MC38 colorectal cancer cells were implanted into the flank of germ-free (GF) or specific-pathogen-free (SPF) mice followed by ICB therapy once tumors were palpable (fig. S2A). Anti-CTLA-4 treatment led to smaller tumors (fig. S2B) and markedly increased intratumoral and splenic CD4+ and CD8+ T cell activation and proliferation in SPF mice compared with GF mice (fig. S2, C to F). To ensure that the lack of ICB efficacy was not merely a reflection of the immature immune system of GF mice, we also assessed the effect of ICB therapy in antibiotic-treated SPF mice (fig. S2G). Similar to what was observed in GF mice, broad-spectrum antibiotics reduced

[1]Department of Physiology and Pharmacology, Snyder Institute of Chronic Diseases, Cumming School of Medicine, University of Calgary, Calgary, Canada. [2]Department of Microbiology, Immunology and Infectious Diseases, Snyder Institute of Chronic Diseases, Cumming School of Medicine, University of Calgary, Calgary, Canada. [3]International Microbiome Centre, Cumming School of Medicine, University of Calgary, Calgary, Canada. [4]Department of Biochemistry and Molecular Biology and Department of Physiology and Pharmacology, Charbonneau Cancer Institute, Alberta Children's Hospital Research Institute, Cumming School of Medicine, University of Calgary, Calgary, Canada. [5]Centre de Recherche du Centre Hospitalier de l'Université de Montréal et Institut du Cancer de Montréal, Québec, Canada. [6]Department of Biological Sciences, University of Calgary, Calgary, Canada.
*Corresponding author. Email: kathy.mccoy@ucalgary.ca (K.D.M.); lukas.mager@ucalgary.ca (L.F.M.)

ICB therapy efficacy in tumor-bearing SPF mice (fig. S2, H to J).

To evaluate whether the isolated bacteria that were enriched in the tumors of ICB-treated mice (Fig. 1G) were able to boost the efficacy of ICB therapy, GF mice were monocolonized with five different isolated bacterial species. MC38 tumor cells were injected heterotopically into monocolonized or GF mice and, upon palpable tumor development, all mice were treated with anti-CTLA-4, after which tumor growth and antitumor immunity were assessed (Fig. 1H). Of the five bacterial species tested, monocolonization with *B. pseudolongum*, *Lactobacillus johnsonii*, and *Olsenella* species
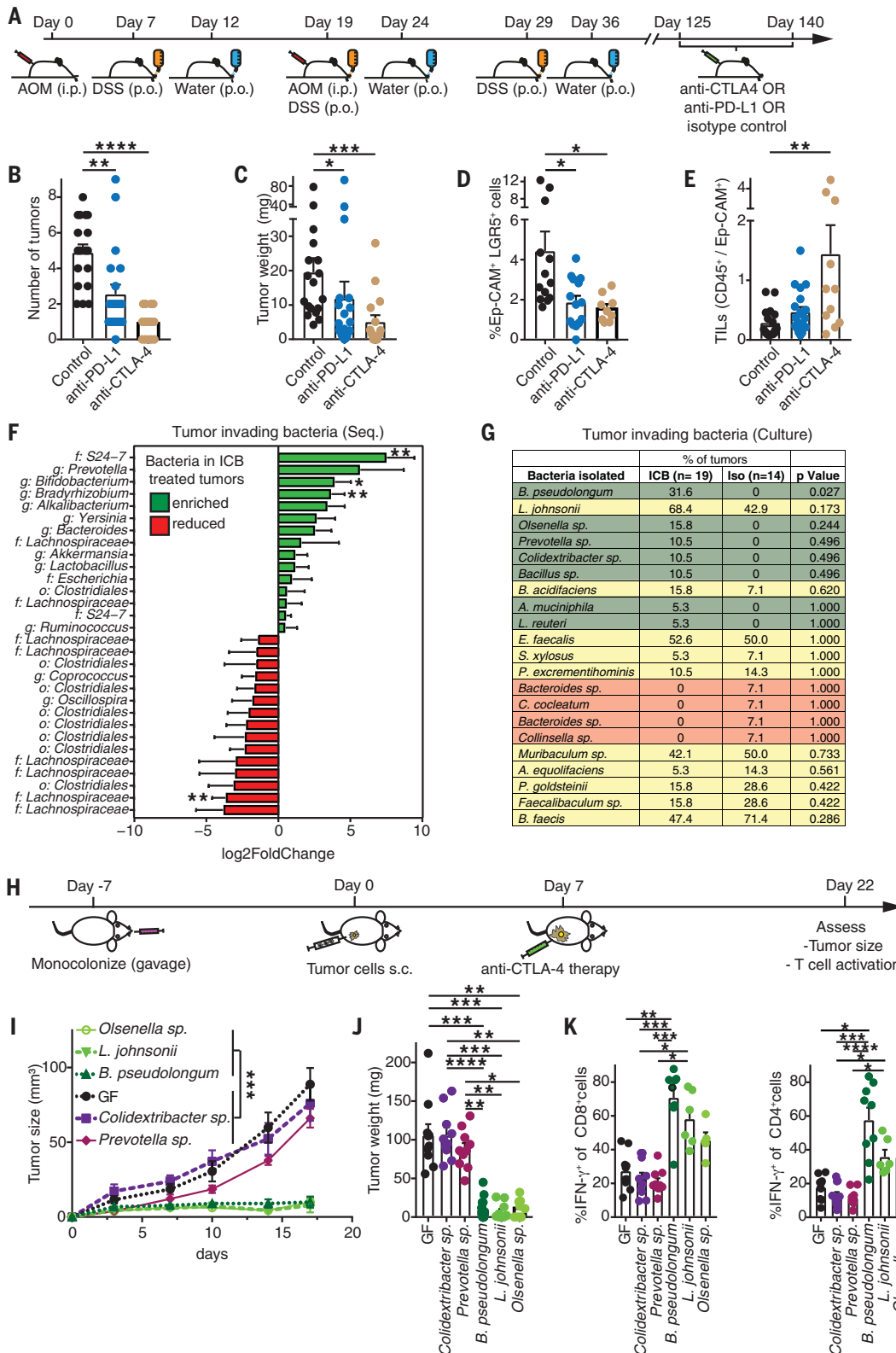

Fig. 1. Identification of bacteria that promote response to ICB therapy. (**A**) Schematic of the experimental setup. Animals were treated with either anti-CTLA-4, anti-PD-L1, or isotype control antibody. i.p., intraperitoneally; p.o., orally. (**B**) Number of tumors, (**C**) tumor weight, (**D**) EpCAM⁺LGR5⁺ cancer stem cells, and (**E**) tumor-infiltrating leukocytes (TILs) of AOM/DSS intestinal tumors in SPF mice after treatment with isotype, anti-PD-L1, or anti-CTLA-4 antibodies. (**F**) 16S rRNA gene V4 region amplicon sequencing to identify bacteria in tumor tissue. Bacteria enriched or reduced in tumors of anti-PD-L1 or anti-CTLA-4 (ICB) compared with isotype-treated animals are shown in green and red, respectively. f, family; g, genus; o, order. (**G**) Bacteria cultured from homogenized tumors under anaerobic conditions from anti-PD-L1 or anti-CTLA-4 (ICB groups) or isotype (Iso group) treated animals. Bacteria isolated only from ICB-treated tumors shown in green, bacteria isolated only from isotype-treated tumors shown in orange, and bacteria isolated from both ICB- and isotype-treated tumors shown in yellow. (**H**) Schematic of the experimental setup. s.c., subcutaneously. (**I**) Tumor growth, (**J**) tumor weight, and (**K**) quantification of intratumoral IFN-γ⁺CD8⁺ and IFN-γ⁺CD4⁺ T cells are shown in GF or mono-colonized (*B. pseudolongum*, *Colidextribacter* species, *L. johnsonii*, *Olsenella* species, or *Prevotella* species) MC38 tumor–bearing mice. Data indicate mean ± SEM [(B) to (E), and (I) to (K)] or mean ± log fold change standard error (F) and are pooled from three individual experiments. [(A) to (E)] *n* = 16 to 20 mice per group. [(H) to (K)] >*n* = 8 to 15 mice per group. **P* < 0.05; ***P* < 0.01; ****P* < 0.001; *****P* < 0.0001.

Fig. 2. Effect of
***B. pseudolongum* and
ICB on T$_H$1 T cell
phenotype and
identification of
the immunotherapy-
promoting metabolite
inosine.** (**A**, **D**, and
F) Schematic of the
experimental setups. i.v.,
intravenously. (**B**) Rep-
resentative plots and
quantification of T-bet$^+$
and T-bet$^+$IFN-γ$^+$ events
of CD3ε$^+$CD4$^+$ cells in
the small intestine
(SI) in the presence of
indicated bacteria at
day 28. (**C**) Same as (B),
but in the spleen.
(**E**) Representative plots
and quantification of
T-bet$^+$IFN-γ$^+$ events of
CD3ε$^+$CD4$^+$ T cells in the
spleen in the presence
of indicated bacteria and
anti-CTLA-4 treatment
at day 32. (**G**) Tumor
growth and (**H**) tumor
weight are shown
32 days after MC38
tumor challenge and
subsequent serum
transfer and anti-CTLA-4
treatment. (**I**) Quantifica-
tion of intratumoral IFN-
γ$^+$CD8$^+$ and IFN-γ$^+$CD4$^+$
T cells. (**J**) Scatter
plot of untargeted
metabolomics data in the
serum of anti-CTLA-4–
treated tumor-bearing
B. pseudolongum–
monocolonized mice
compared with
Colidextribacter species–
monocolonized and
GF mice. Red circles
or dotted red circles
depict inosine or
inosine fragments and
adducts, respectively.
Inset shows an
extracted ion

chromatogram of inosine. *m/z*, mass to charge ratio; au, arbitrary units. (**K**) Intensity of inosine (AUC, area under the curve) in sera shown in (J). Data indicate mean ± SEM and are pooled from two individual experiments. [(A) to (E)] *n* = 10 or 11 mice per group. [(F) to (K)] *n* = 5 to 8 mice per group. *P < 0.05; **P < 0.01; ***P < 0.001; ****P < 0.0001.
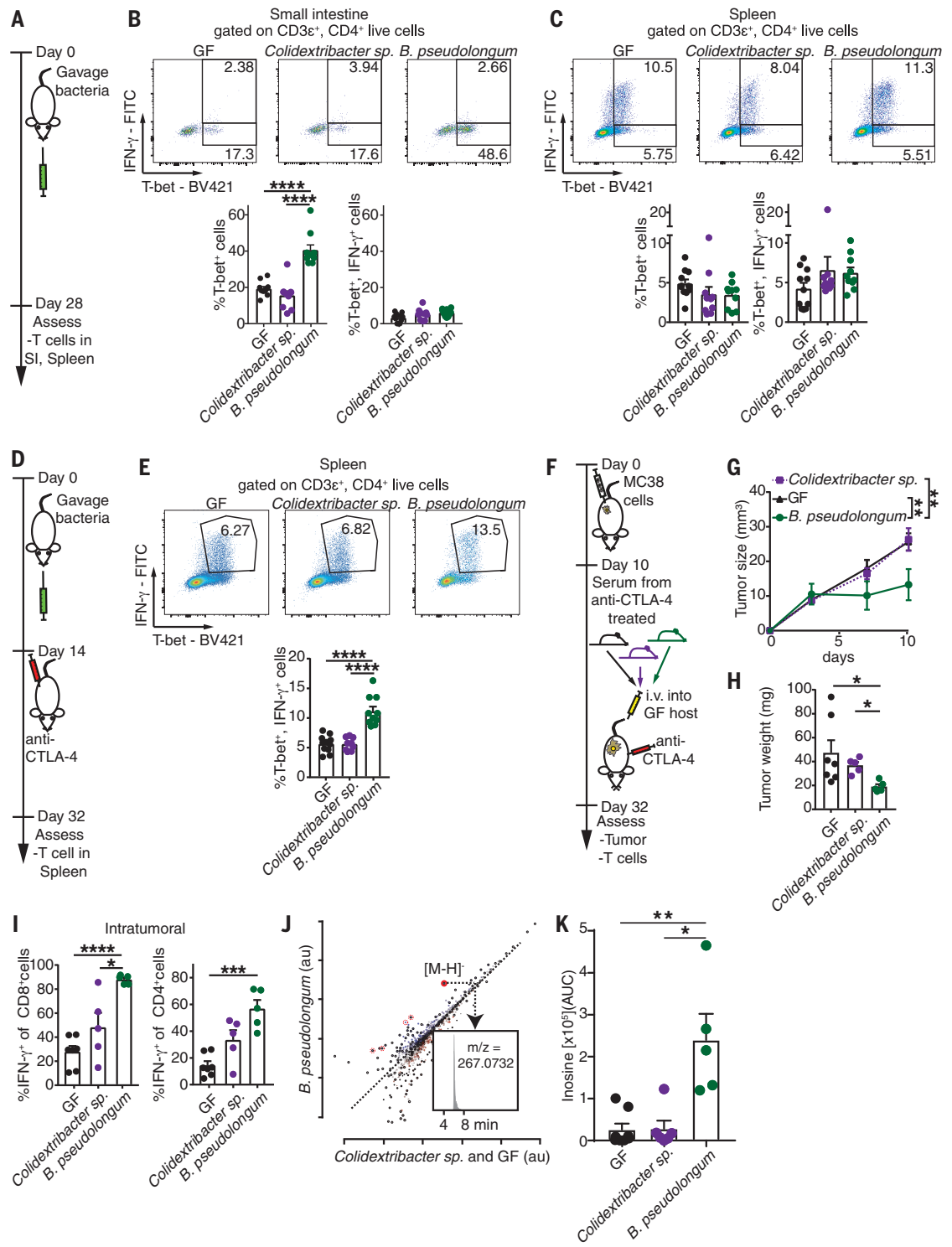
significantly enhanced the efficacy of anti-CTLA-4 treatment compared with GF mice or mice monocolonized with *Colidextribacter* species or *Prevotella* species (Fig. 1, I and J, and fig. S3, A and B). In addition, CD4$^+$ and CD8$^+$ T cell activation was substantially increased (Fig. 1K), whereas proliferation of intratumoral CD8$^+$ T cells (fig. S3, C and D) was modestly increased in the tumors of *B. pseudolongum*, *L. johnsonii*, and *Olsenella* species–monocolonized animals.

The isolated ICB-promoting *B. pseudolongum* strain also improved the efficacy of anti-PD-L1 treatment in the MC38 heterotopic tumor model compared with the *Colidextribacter* species control bacteria (fig. S4), albeit to a lesser

extent than that observed for anti-CTLA-4 treatment (at the same dose), similar to our observations in the AOM/DSS model. Because *B. pseudolongum* provided the most robust ICB-promoting effect, it was selected for further mechanistic studies. Note that other *Bifidobacterium* species, such as *B. breve* and *B. longum*, have previously been found to promote antitumor immunity and enhance anti-PD-L1 efficacy in a murine model of melanoma (7). In humans, *B. longum* has been reported to be enriched in anti-PD-1 responders (9). Furthermore, *B. pseudolongum* species are widely distributed in the mammalian gut, with many different strains displaying genomic diversity and differential metabolic capacities (19), suggesting strain-dependent functions.

We found that antitumor immunity was dependent on ICB therapy, as monocolonization with *B. pseudolongum* in the absence of anti-CTLA-4 treatment was not able to reduce tumor growth (fig. S5, A to C) or induce antitumor immunity (fig. S5, D and E), which is similar to previous studies with other ICB-promoting bacteria (6, 8). And although previous studies have shown that some bacteria accumulate in the tumor environment, where they locally stimulate the immune system and kill tumor cells through toxic metabolites (20), we could not detect *B. pseudolongum* within the heterotopic tumors (fig. S6). Therefore, despite the fact that *B. pseudolongum* was initially isolated from intestinal tumors, the presence of bacteria within tumors was not required for the enhancement of ICB therapy in our model, suggesting the potential involvement of soluble factors.

Although *B. pseudolongum* did not induce antitumor immunity in the absence of ICB therapy (fig. S5), intestinal *B. pseudolongum* did induce a significant increase in expression of the T helper cell 1 (T_H1) master transcription regulator T-bet in small intestinal lamina propria CD4+ T cells, which was not observed in GF or *Colidextribacter* species monocolonized mice (Fig. 2, A and B). Induction of T-bet illustrated that *B. pseudolongum* has immunomodulatory capacity even in the absence of ICB. In its absence, the immunomodulatory effect was restricted to the gut-associated lymphoid tissue (GALT) and was also observed, albeit to a lesser extent, in the mesenteric lymph nodes (MLN) (fig. S7A), but it was not observed in the spleen (Fig. 2C). In the absence of ICB, *B. pseudolongum* did not increase the activation of effector function of T_H1 cells, as IFN-γ+T-bet+ cells did not differ from controls in any of the tissues assessed (Fig. 2, B and C, and fig. S7A). Thus, in the absence of tumors and ICB therapy, *B. pseudolongum* promoted mucosal T_H1 transcriptional differentiation in GALT without increasing effector function in the gut and draining lymph nodes. While

B. pseudolongum had no effect on other CD4+ T cell subsets in the small intestine (fig. S7B), it did increase CD8+T-bet+ T cells (fig. S7C). Moreover, *B. pseudolongum* had a minimal effect on T_H17 cells and T_{regs} in the MLN and spleen (fig. S7, D to G).

Because *B. pseudolongum* monocolonization in the absence of tumors and ICB therapy induced only local mucosal T_H1 differentiation during homeostasis, we next asked whether the combination of *B. pseudolongum* and anti-CTLA-4 therapy (in the absence of a tumor) would lead to systemic T_H1 activation. Indeed, colonization with *B. pseudolongum* combined with ICB treatment led to significantly enhanced splenic T_H1 cell activation and effector function, as evidenced by IFN-γ production compared with *Colidextribacter* species–monocolonized or GF animals (Fig. 2, D and E, and fig. S7, H and I). We concluded that *B. pseudolongum* induces T_H1 differentiation and, together with anti-CTLA-4, activation of T_H1 effector T cells. Interestingly, a recently defined consortium of 11 bacteria (which did not include any *Bifidobacterium* spp.) induced IFN-γ production preferentially in CD8+ T cells and promoted antitumor immunity in the absence of immunotherapy (21). In contrast, *B. pseudolongum* induced IFN-γ production in both CD4+ and CD8+ T cells (fig. S7J), and ICB treatment was required for antitumor immunity.

We were intrigued by the ability of *B. pseudolongum* to induce T_H1 transcriptional differentiation during homeostasis as opposed to activation of T_H1 effector function after ICB treatment. Gastrointestinal inflammation is a common immune-related adverse effect of anti-CTLA-4 treatment (1), and we reasoned that this may be due to alterations in gut barrier integrity. Indeed, monocolonized animals treated with anti-CTLA-4 displayed increased systemic serum anticommensal antibody reactivity, particularly T_H1-associated immunoglobulin G2b, and reduced small intestinal transepithelial electrical resistance compared with controls (fig. S8, A and B). Despite this, anti-CTLA-4 treatment did not induce overt local or systemic inflammation (fig. S8, C and D). In this regard, it is notable that some *Bifidobacterium* species have been reported to provide protection from anti-CTLA-4–induced enterocolitis with no effect on tumor growth (22). The induction of systemic antibacterial antibodies after ICB therapy was not required for the ICB-promoting effect, as anti-CTLA-4 treatment was also effective in *B. pseudolongum*–monocolonized mice deficient in B cells and antibodies (fig. S9). Therefore, because bacteria did not accumulate in (heterotopic) tumors (fig. S6), anti-CTLA-4 reduced the integrity of the gut barrier (fig. S8), and B cells and anticommensal antibodies were not required for the ICB-promoting effect of *B. pseudolongum* (fig. S9), we hypothesized that increased systemic

translocation of metabolites may be responsible for the systemic effect of *B. pseudolongum* during ICB therapy. To address this hypothesis, serum collected from tumor-bearing GF, *B. pseudolongum*, or *Colidextribacter* species–monocolonized mice treated with anti-CTLA-4 was transferred concomitantly with anti-CTLA-4 into GF MC38 tumor–bearing mice (Fig. 2F). Unexpectedly, serum from anti-CTLA-4–treated *B. pseudolongum* monocolonized mice, but not serum from anti-CTLA-4–treated GF or *Colidextribacter* species–monocolonized mice, was sufficient to reduce tumor growth and elicit strong antitumor immunity in the tumor and spleen of GF mice (Fig. 2, G to I, and fig. S10). Together, these data show that soluble factors derived from, or induced by, *B. pseudolongum* were responsible for the observed ICB-promoting effects.

Untargeted metabolomics of the serum samples revealed increased levels of several metabolites in sera from *B. pseudolongum* compared with *Colidextribacter* species–monocolonized and GF mice (Fig. 2J and fig. S11, A and B). Notably, the purine metabolite inosine was the only metabolite that was significantly more abundant (eight to ninefold) in sera from *B. pseudolongum*–monocolonized mice compared with sera from *Colidextribacter* species–monocolonized or GF mice (Fig. 2K). Of note, xanthine and hypoxanthine, degradation products of inosine, were also elevated in the sera of *B. pseudolongum*–monocolonized mice (table S1). Analysis of bacterial culture supernatant revealed that both *B. pseudolongum* and *A. muciniphila* produced significantly higher amounts of inosine than did *Colidextribacter* species under the same culture conditions (fig. S11C), revealing that inosine is a bacterial metabolite produced by *B. pseudolongum* and *A. muciniphila*. In contrast, although *L. johnsonii* did not produce inosine, it did produce large amounts of hypoxanthine—a potent ligand binding to the same receptor as inosine—compared with *Colidextribacter* species (fig. S11D) (23). Inosine monophosphate and hypoxanthine were two of the most elevated metabolites in the cecum and serum of mice colonized with the consortium of 11 bacteria that Tanoue *et al.* recently identified to improve ICB therapies (21). The identity of inosine was confirmed by fragmentation analysis (fig. S11E).

To determine the physiological inosine levels in vivo, we measured inosine concentrations in duodenal, jejunal, and cecal contents of *B. pseudolongum*–monocolonized mice. Inosine concentrations were highest in the duodenum and gradually decreased along the gastrointestinal tract [duodenum (66.13 ± 14.23 μM) > jejunum (29.26 ± 9.38 μM) > cecum (0.5 ± 0.05 μM)] (fig. S11F). We also quantified inosine concentrations in the serum of anti-CTLA-4– and anti-PD-L1–treated *B. pseudolongum*
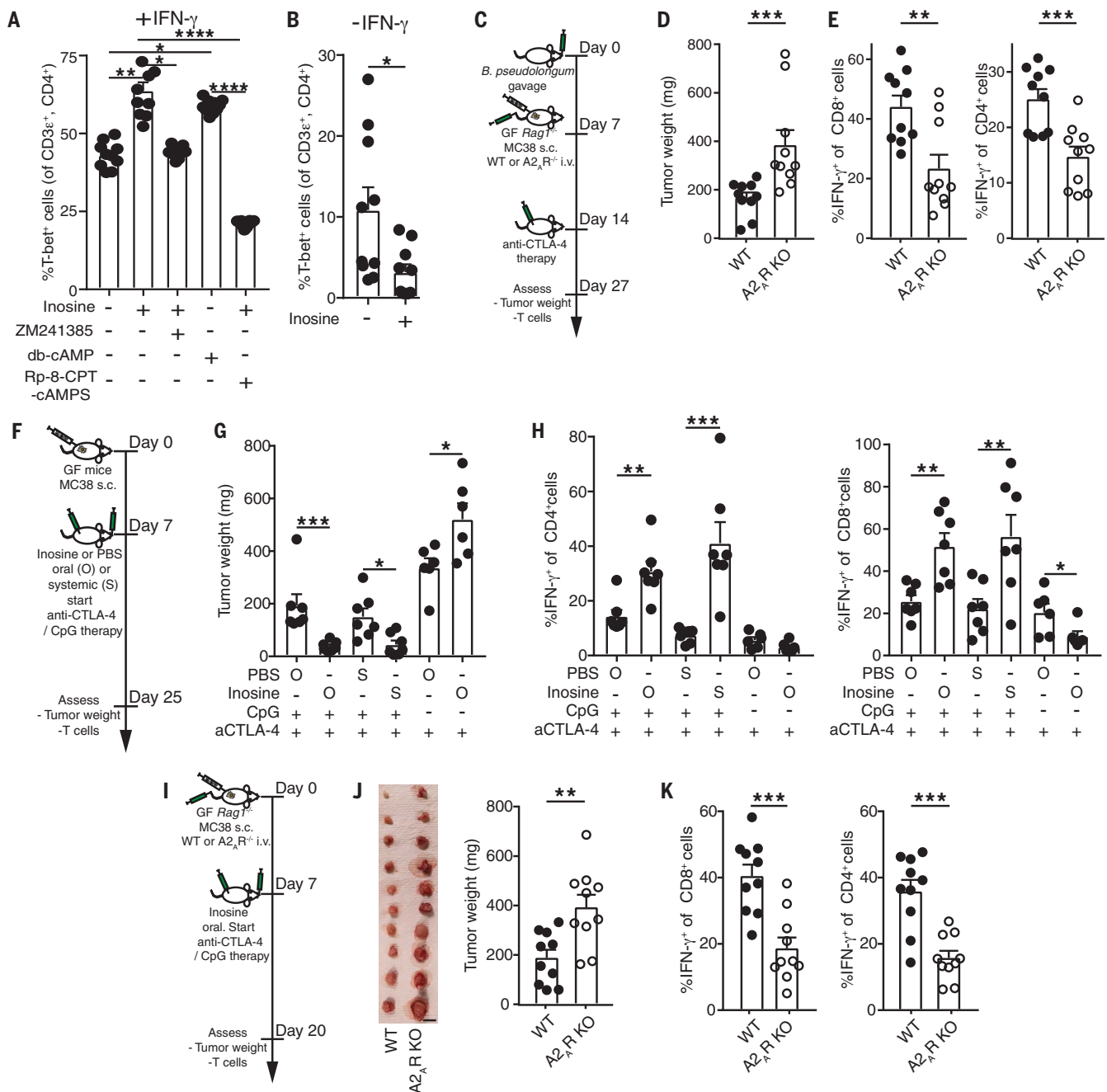
Fig. 3. Inosine promotes T$_H$1 activation and antitumor immunity. (**A**) Naïve CD4$^+$ T cells were cocultured with BMDCs and IFN-γ. Quantification of T-bet$^+$CD3$^+$CD4$^+$ T cells 48 hours after coculture in the presence or absence of inosine, A$_{2A}$ receptor inhibitor (ZM241385), cell-permeable cAMP (db-cAMP), and protein kinase A inhibitor (RP-8-CPT-cAMPS). (**B**) Same as (A), but without IFN-γ. (**C**) Schematic overview to assess the requirement of A$_{2A}$R signaling for *B. pseudolongum*–induced antitumor immunity. GF Rag-1–deficient mice were gavaged with *B. pseudolongum* and 7 days later 1 × 10^6 MC38 cells (s.c.) and wild-type (WT) or A$_{2A}$R-deficient 1 × 10^7 T cells (i.v. 6 × 10^6 CD4$^+$ and 4 × 10^6 CD8$^+$ T cells) were injected. Upon development of palpable tumors, mice were treated with 100 μg anti-CTLA-4 (four times every 72 hours). (**D**) Tumor weight and (**E**) quantification of IFN-γ$^+$ in CD8$^+$ or CD4$^+$ T cells in the tumor are shown. (**F**) Schematic overview of experimental setup to assess the effect of inosine on antitumor immunity. Upon development of palpable tumors, mice were treated with 100 μg anti-CTLA-4 i.p. (five times every 72 hours) and in

some groups 20 μg CpG i.p. (five times every 72 hours). In addition, inosine (300 mg per kilogram of body weight) or PBS was given daily orally (O) through gavage or systemically (S) through i.p. injection. (**G**) Tumor weight and quantification of intratumoral IFN-γ$^+$ cells among (**H**) CD4$^+$ or CD8$^+$ T cells are shown. (**I**) Schematic overview to assess the requirement of A$_{2A}$R signaling for inosine-induced antitumor immunity. GF Rag1$^{-/-}$ mice were injected with 1 × 10^6 MC38 cells (s.c.) and WT or A$_{2A}$R-deficient 1 × 10^7 T cells (i.v. 6 × 10^6 CD4$^+$ and 4 × 10^6 CD8$^+$ T cells). Upon development of palpable tumors, mice were treated with 100 μg anti-CTLA-4, 20 μg CpG (four times every 72 hours, both i.p.) and inosine (daily, 300 mg per kilogram of body weight, through gavage). (**J**) Pictures of tumors and tumor weight are shown at day 20. KO, knockout. Scale bar, 1 cm. (**K**) Quantification of IFN-γ$^+$ in CD8$^+$ or CD4$^+$ T cells in the tumor are shown. Data indicate mean ± SEM, pooled from two individual experiments. [(A) and (B)] n = 10 biological replicates per group. [(C) to (K)] n = 6 to 10 mice per group. *P < 0.05; **P < 0.01; ***P < 0.001; ****P < 0.0001.

(anti-CTLA-4: 26.16 ± 3.32 μM; anti-PD-L1: 37.5 ± 10.2 μM) and *Colidextribacter* species (anti-CTLA-4: 3.26 ±1.01 μM; anti-PD-L1: 4.8 ± 1.3 μM) monocolonized mice (fig. S11F), in the serum of SPF mice before (4.08 ± 1.12 μM) and after anti-CTLA-4 treatment (11.65 ± 2.09 μM) and in the serum of antibiotic-treated SPF mice given anti-CTLA-4 (2.03 ± 0.86 μM) (fig. S11G). These data indicated that bacterial production of inosine in the upper gastrointestinal tract is likely to be the predominant source of elevated systemic inosine levels in *B. pseudolongum* monocolonized mice.

The identification of inosine was initially surprising because inosine binds to the adenosine 2A receptor ($A_{2A}R$), which has been demonstrated to inhibit T_H1 differentiation in vitro and antitumor immunity in vivo (*24–27*). Data supporting an immunosuppressive role for adenosine and $A_{2A}R$ signaling have led to the development of novel immune checkpoint inhibitor targets, such as monoclonal antibody–targeting CD73, CD39, and CD38 and pharmacological antagonists of $A_{2A}R$, many of which are currently in clinical trials [reviewed in (*28*)]. However, a small body of literature has demonstrated that inosine analogs can be proinflammatory and that $A_{2A}R$ signaling can sustain T_H1 and antitumor immunity in mice (*29–31*). On the basis of these opposing findings, we investigated whether inosine could enhance T_H1 cell differentiation in vitro. Activated ovalbumin 323-339 ($OVA_{323-339}$) peptide-pulsed bone marrow–derived dendritic cells (BMDCs) were cocultured with naïve $OVA_{323-339}$-specific OT-II $CD4^+$ T cells in the presence or absence of inosine. The effect of inosine in terms of induction or inhibition of $CD4^+$ T_H1 T cell differentiation turned out to be context dependent. Specifically, in the presence of exogenous IFN-γ, inosine strongly boosted T_H1 differentiation of naïve T cells (Fig. 3A), whereas in the absence of IFN-γ, inosine inhibited T_H1 differentiation (Fig. 3B and fig. S12A). We next dissected the molecular mechanism through which inosine enhanced T_H1 differentiation. Whereas the pharmacological inhibition of $A_{2A}R$ signaling (with the high affinity antagonist ligand ZM241385) completely abrogated the effect of inosine, the addition of cell-permeable dibutyryl–cyclic adenosine monophosphate (db-cAMP), a signaling molecule downstream of $A_{2A}R$, restored T_H1 differentiation and bypassed the need for inosine (Fig. 3A). Furthermore, inhibition of protein kinase A (PKA), a downstream effector molecule of cAMP, negated inosine-driven T_H1 differentiation (Fig. 3A). In addition, the inosine-$A_{2A}R$-cAMP-PKA signaling cascade led to phosphorylation of the transcription factor cAMP response element–binding protein (CREB) (fig. S12B), a known

transcriptional enhancer of key T_H1 differentiation factors, such as interleukin-12 (IL-12) receptor and IFN-γ (*32–34*). We also observed inosine-dependent up-regulation of the IL-12 receptor, beta 2 subunit (IL12Rβ2) (fig. S12C).

The effect of inosine was T cell–intrinsic, because the addition of inosine to naïve T cells that had been activated with anti-CD3– and anti-CD28–coated beads also enhanced T_H1 differentiation, even in the absence of IFN-γ (fig. S12D). Furthermore, induction of T_H1 differentiation and phosphorylation of CREB was absent when $A_{2A}R$-deficient T cells were stimulated with inosine (fig. S12, E and F). In contrast, bypassing the need for $A_{2A}R$ signaling by using db-cAMP increased T_H1 differentiation and phosphorylation of CREB in $A_{2A}R$-deficient T cells, confirming that the T_H1 promoting effect of inosine is dependent on $A_{2A}R$ signaling (fig. S12, E and F). Additionally, given that phosphorylated CREB is known to bind to key T_H1 target genes, we confirmed that inosine stimulation led to a sustained up-regulation of *Il12rb2* and *Ifng* gene expression in $CD4^+$ T cells (fig. S12, G and H). Inosine dose response experiments revealed that the physiological concentrations of inosine observed in sera of *B. pseudolongum* but not *Colidextribacter* species–monocolonized mice were sufficient to induce T_H1 activation (fig. S12I). In contrast, adenosine, which also binds to the $A_{2A}R$, was present only at extremely low levels in intestinal contents, and serum levels did not differ between *B. pseudolongum* and *Colidextribacter* species–monocolonized mice (fig. S12J), indicating that adenosine was unlikely to be mediating the ICB-promoting effects of *B. pseudolongum*. Furthermore, adenosine dose-response experiments revealed that the levels of adenosine in the serum were insufficient to promote T_H1 activation and effector function (fig. S12K). To confirm whether the inosine-mediated T_H1 promoting effect in vitro also applied to in vivo conditions, GF mice were immunized with ovalbumin in combination with CpG as a costimulus. Note that we used CpG as a costimulus because it is a widely used antitumor adjuvant in different settings [reviewed in (*35*)]. One day later, mice received inosine or vehicle by intraperitoneal administration. Inosine increased the proportions of T-bet$^+$IFN-γ$^+$CD8$^+$ and T-bet$^+$IFN-γ$^+$CD4$^+$ T cells in the MLN (fig. S12, L to N), validating our in vitro results.

We next determined whether the ICB-enhancing ability of *B. pseudolongum* required $A_{2A}R$ expression specifically on T cells. Antitumor immunity was assessed in *B. pseudolongum* monocolonized *Rag1*-deficient mice bearing MC38 tumors that had been adoptively transferred with either $A_{2A}R$-deficient or wild-type T cells and treated with anti-CTLA-4 (Fig. 3C). We found that the absence of $A_{2A}R$ expression

on T cells reduced the ICB-promoting effect of *B. pseudolongum* (Fig. 3, D and E).

We then determined whether inosine could promote antitumor immunity induced by anti-CTLA-4 in the absence of *B. pseudolongum*. GF mice were challenged with MC38 tumor cells and upon development of palpable tumors, inosine or phosphate-buffered saline (PBS) was given orally or systemically in combination with anti-CTLA-4 treatment and CpG as a costimulus (Fig. 3F). Compared with PBS, both oral and systemic administration of inosine led to reduced tumor weights and increased antitumor immunity when given together with anti-CTLA-4 and CpG (Fig. 3, G and H). But in the absence of CpG, inosine increased tumor weight and reduced antitumor immunity (Fig. 3, G and H), validating our previous in vitro findings demonstrating that the effect of inosine was context-dependent and based on the presence or absence of costimulation. Inosine-induced antitumor immunity was also dependent on $A_{2A}R$ signaling in T cells, as oral supplementation with inosine failed to induce antitumor immunity in MC38 tumor–bearing GF *Rag1*-deficient animals adoptively transferred with $A_{2A}R$-deficient T cells (Fig. 3, I to K). These data indicated that the ICB-promoting effect of *B. pseudolongum* was mediated by inosine and was dependent on $A_{2A}R$ signaling specifically in T cells.

Because we detected *A. muciniphila*—a species that was previously shown to increase ICB therapy efficacy (*8*) and to produce inosine in vitro (fig. S11C)—in ICB-treated tumors (Fig. 1G), we further investigated whether *A. muciniphila* also relies on $A_{2A}R$ signaling to enhance ICB-therapy efficacy. We found that monocolonization with *A. muciniphila* in combination with anti-CTLA-4 led to smaller tumors and increased antitumor immunity, and this was dependent on T cell expression of $A_{2A}R$ (fig. S13, A to D). Although monocolonization with *L. johnsonii* was able to promote the antitumor effects of anti-CTLA-4 (Fig. 1, I to K, and fig. S5), hypoxanthine (another ligand of the $A_{2A}R$), not inosine, was elevated in in vitro cultures (fig. S11, C and D). Despite this, the ICB-promoting effect of *L. johnsonii*, although less potent than that of *B. pseudolongum* and *A. muciniphila*, was also partially dependent on T cell expression of $A_{2A}R$ (fig. S13, E to H).

We next tested whether inosine could also promote the efficacy of anti-CTLA-4 therapy in the presence of a complex microbiota. We first used a gnotobiotic model where mice are stably colonized with a defined microbiota consisting of 12 bacterial species, referred to as Oligo-Mouse-Microbiota-12 (Oligo-MM^{12}) (*36*), which lacks *B. pseudolongum*. We found that inosine was able to promote the antitumor effects of anti-CTLA-4, with reduced

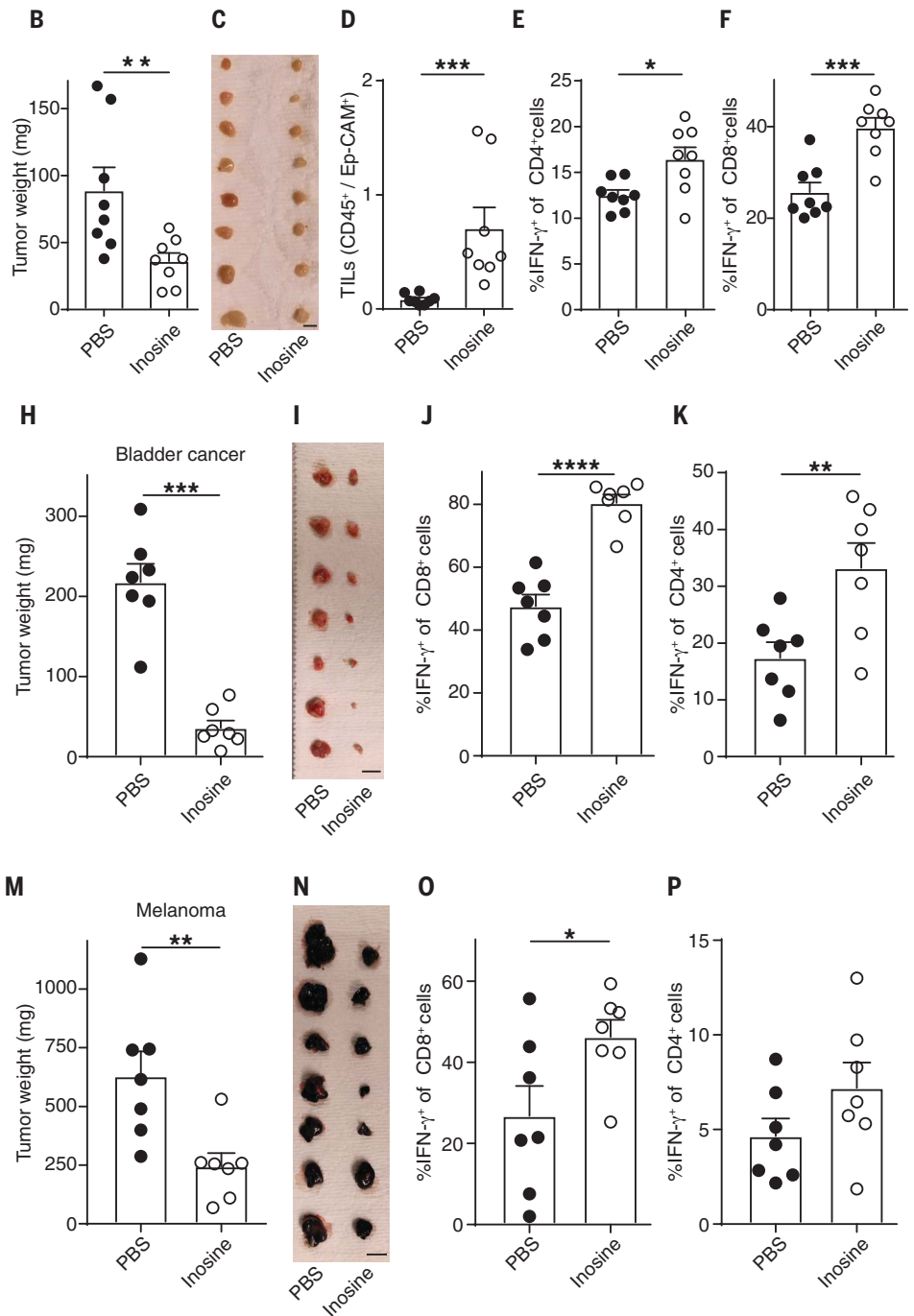**Fig. 4. The metabolite inosine promotes immunotherapy response in mouse models of intestinal cancer, bladder cancer, and melanoma.** (**A**) Schematic overview of experimental setup to assess the effect of inosine in SPF *Msh2^{LoxP/LoxP}Villin-Cre* mice. On day 312, mice received antibiotics orally (ampicillin, 1 mg/ml; colistin, 1 mg/ml; and streptomycin, 5 mg/ml) until the end of the experiment, and on day 319 mice received 100 μg anti-CTLA-4 i.p. and 20 μg CpG i.p. (both five times every 72 hours) and PBS or inosine (300 mg per kilogram of body weight) orally through gavage daily. (**B**) Tumor weight, (**C**) representative pictures of dissected tumors, (**D**) quantification of TILs and splenic IFN-γ^+ production of (**E**) CD4^+ and (**F**) CD8^+ T cells is shown. (**G**) Schematic overview of experimental setup to assess the effect of inosine on bladder cancer. GF animals were subcutaneously injected in the flank with 2 × 10^6 MB49 bladder cancer cells. Upon development of palpable tumors, mice were treated with 100 μg anti-CTLA-4 i.p. and 20 μg CpG i.p. (three times every 72 hours) and PBS or inosine (300 mg per kilogram of body weight) orally through gavage daily. (**H**) Tumor weight and (**I**) pictures of tumors are shown. Quantification of IFN-γ^+ in (**J**) CD8^+ or (**K**) CD4^+ cells in the tumor are shown. (**L**) Schematic overview of experimental setup to assess the effect of inosine on melanoma. GF animals were subcutaneously injected in the flank with 1 × 10^6 B16-F10 melanoma cells. Upon development of palpable tumors, mice were treated with 100 μg anti-CTLA-4 i.p. and 20 μg CpG i.p. (three times every 72 hours) and PBS or inosine (300 mg per kilogram of body weight) orally through gavage daily. (**M**) Tumor weight and (**N**) pictures of tumors are shown. Quantification of IFN-γ^+ in (**O**) CD8^+ or (**P**) CD4^+ cells in the tumor are shown. Data indicate mean ± SEM. [(A) to (F)] $n = 8$ mice per group. [(G) to (P)] $n = 7$ mice per group. *$P < 0.05$; **$P < 0.01$; ***$P < 0.001$, ****$P < 0.0001$. All scale bars, 1 cm.

tumor size and increased intra-tumoral IFN-γ^+CD8^+ and IFN-γ^+CD4^+ T cells even in gnotobiotic Oligo-MM^12 mice (fig. S14, A to D). We also found that inosine could promote the efficacy of anti-CTLA-4 in SPF mice, which contain a highly diverse microbiota (fig. S14, E to H). We then examined whether

B. pseudolongum needed to be viable to enhance anti-CTLA-4 efficacy. Whereas gavage of live *B. pseudolongum*, with or without antibiotic pretreatment, enhanced anti-CTLA-4 effects in SPF mice (fig. S14, E to H), heat-killed *B. pseudolongum* was unable to boost the effects of ICB therapy, likely because of

the inability to produce inosine (fig. S14, E to H).

In addition to direct stimulation of T cells, inosine could potentially affect tumor cells directly through altering tumor cell survival or susceptibility to T cell–mediated killing. However, direct in vitro exposure of MC38

tumor cells to inosine did not modulate tumor cell viability (fig. S15A), and pretreatment of MC38 tumor cells before coculture with activated tumor-specific T cells did not promote or inhibit T cell–mediated killing of tumor cells (fig. S15B), further supporting the conclusion that the antitumor effect of inosine was mediated primarily through T cells.

Together, these data indicate that the effect of inosine on T cells required sufficient costimulation (likely by DCs), IL-12 receptor engagement for T_H1 differentiation, and IFN-γ production for efficient antitumor immunity. Indeed, conventional dendritic cells (cDCs), not macrophages, were found to be the primary source of IL-12 (fig. S16, A and B). To further assess the role of cDCs in ICB-bacteria cotherapy, bone marrow (BM) cells from cDC-DTR mice (DTR, diphtheria toxin receptor) were transferred into lethally γ-irradiated recipient SPF mice to allow for inducible, conditional depletion of cDCs. After BM reconstitution, mice were treated with antibiotics and gavaged with a mixture of the three previously identified ICB-promoting bacteria: *B. pseudolongum*, *L. johnsonii*, and *Olsenella* species. Ten weeks later, mice were implanted with MC38 cells and when palpable tumors were established, cDCs were depleted by injection of diphtheria toxin followed by anti-CTLA-4 treatment (fig. S16C). Depletion of cDCs led to larger tumors (fig. S16D), a significant reduction in intratumoral CD8$^+$ and CD4$^+$ T cell frequencies and IFN-γ production (fig. S16E), and markedly reduced IFN-γ production and proliferation of splenic CD8$^+$ and CD4$^+$ T cells (fig. S16F). Therefore, depletion of cDCs strongly impeded the ability of the bacteria-elicited ICB response to reduce established tumors, which indicated the requirement for continuous antigen presentation, IL-12 production, and T cell costimulation by cDCs for efficient ICB therapy. The critical involvement of cDC and IL-12 has previously been reported for anti-PD-1 treatment (37).

Because enhanced T_H1 immunity is generally considered to be beneficial for most antitumor responses [reviewed in (38)], we next determined whether intestinal colonization with the isolated ICB-promoting bacteria or treatment with inosine would be equally effective in other tumor models. First, we tested the ICB-promoting effect of *B. pseudolongum*, *L. johnsonii*, and *Olsenella* species in SPF $Msh2^{LoxP/LoxP}Villin-Cre$ (39) animals that have conditional inactivation of *Msh2* (a DNA mismatch repair gene) in intestinal epithelial cells and develop adenocarcinomas in the small intestine. Previous reports have shown greater efficacy of ICB in mismatch repair–deficient (MMRD) cancer in the clinical setting (15, 40). In the $Msh2^{LoxP/LoxP}Villin-Cre$ model, anti-

CTLA-4 treatment alone (without the addition of ICB-promoting bacteria) led to reduced tumor weights and EpCam$^+$Lgr5$^+$ cells in the tumor, markers for epithelial cell stemness, and increased T cell activation and immune cell infiltration in the tumor (fig. S17, A to F). Cotreatment with ICB-promoting bacteria markedly boosted the effect of anti-CTLA-4 (fig. S17G), leading to a further reduction of tumor weight and EpCam$^+$Lgr5$^+$ cells together with drastically enhanced T cell activation and immune cell infiltration in the tumor compared with control bacteria (fig. S17, H to L). These results suggested that bacterial cotherapy may optimize treatment regimens in MMRD tumors. Notably, anti-IL-12p75 treatment almost completely abrogated the effect of ICB-promoting, anti-CTLA-4 cotherapy in $Msh2^{LoxP/LoxP}Villin-Cre$ tumors (fig. S17, G to L), which supports a critical role for inosine-dependent up-regulation of IL12Rβ2 on T cells and cDC production of IL-12 and corroborates similar findings upon simultaneous depletion of IL-12 and IL-23, using anti-IL-12p40 treatment (6, 8). As oxaliplatin and anti-PD-L1 cotreatment is a more commonly used therapy in clinics, we also confirmed that ICB-promoting bacteria enhanced the efficacy of oxaliplatin and anti-PD-L1 cotreatment in SPF $Msh2^{LoxP/LoxP}Villin-Cre$ animals (fig. S18).

As *B. pseudolongum* was enriched in AOM/DSS tumors of ICB-treated animals (Fig. 1, F and G), and *Bifidobacteria* were previously associated with improved ICB-therapy efficacy in cancer patients (9), we wondered whether *Bifidobacteria* were also enriched in $Msh2^{LoxP/LoxP}Villin-Cre$ tumors of ICB-treated mice. While the total amount of tumor-associated bacteria did not change with anti-CTLA-4 or anti-PD-L1 treatment (fig. S19A), ICB treatment led to specific enrichment of tumor-associated *Bifidobacteria* (fig. S19B). A recent report revealed that, compared with other tissues, *Bifidobacteria* colonize tumors, likely owing to the hypoxic environment often found in tumors (41). At this point, it is unclear why *Bifidobacteria* seem to preferentially accumulate in ICB-treated conditions.

We next tested the ICB-promoting effect of *B. pseudolongum*, *L. johnsonii*, and *Olsenella* species in SPF $Apc^{2lox14/+};Kras^{LSL-G12D/+};Fabpl-Cre$ (42) mice, which have conditional *Apc* deficiency and activation of *Kras* specifically in colonocytes. In this model of CRC, anti-CTLA-4 treatment did not improve survival compared with isotype-treated animals (fig. S20, A and B), and transfer of the ICB-promoting bacteria failed to enhance survival (fig. S20, C and D), revealing a limitation of bacterial cotherapy in this model.

Finally, we tested whether the bacterial metabolite inosine in combination with costimulation was sufficient to enhance the ef-

ficacy of ICB therapy in other cancer models. Oral administration of inosine together with anti-CTLA-4 and CpG treatment in SPF $Msh2^{LoxP/LoxP}Villin-Cre$ mice led to significant reduction in tumor weight and a corresponding increase in splenic IFN-γ$^+$CD4$^+$ and IFN-γ$^+$CD8$^+$ T cells (Fig. 4, A to F). Notably, inosine together with CpG was also found to be effective in promoting the efficacy of anti-CTLA-4 in two additional murine cancers—bladder cancer and melanoma. Specifically, inosine plus CpG administration to GF mice that had been injected with MB49 murine bladder cancer cells was able to significantly enhance the ability of anti-CTLA-4 to reduce tumor weight and increase the proportion of IFN-γ$^+$CD4$^+$ and IFN-γ$^+$CD8$^+$ T cells infiltrating the tumors (Fig. 4, G to K). Similarly, inosine plus CpG augmented the ability of anti-CTLA-4 to mediate antitumor immunity in a heterotopic mouse model of melanoma (Fig. 4, L to P).

Our results identify a *B. pseudolongum* strain isolated from ICB-treated CRC tumors as a key commensal intestinal bacterial species that is capable of boosting a cDC-dependent T_H1 cell circuit to greatly enhance the effect of ICB therapies in mouse models of intestinal and epithelial tumors (fig. S21). These data support the premise that modification of the microbiota or targeted bacterial therapies with defined microbial consortia may provide a promising adjuvant therapy to ICB in CRC and other cancers. Although isolated from mice, all three ICB-promoting bacteria are also found in humans, indicating their potential for translation (43–45). Furthermore, we analyzed published human fecal microbiome metagenomic datasets (8, 9, 46) and found a trend, although not significant, where *B. pseudolongum* was enriched [up to 2.4-fold (8)] in responders compared with nonresponding cancer patients (fig. S22A). At the genus level, *Bifidobacteria* were also enriched (albeit nonsignificantly) in responders compared with nonresponders [5.9-fold (9)] (fig. S22B), with the species *B. longum* and *B. adolescentis* significantly enriched (47). Owing to the low abundance of *B. pseudolongum* in fecal samples of adults, higher-powered studies with larger sample sizes will be needed to confirm this trend. We also identified inosine as a key bacterial-derived metabolite acting through T cell–specific A$_{2A}$R signaling to promote T_H1 cell activation in a context-dependent manner. We further confirmed that *A. muciniphila*, which is known to be associated with responsiveness to ICB therapy in humans (8), uses inosine-A$_{2A}$R signaling for its ICB-promoting effect. In light of our findings, one might caution against the blockade of inosine-A$_{2A}$R signaling for cancer immunotherapy, as this may negate any positive effect provided by beneficial microbes. We suggest that A$_{2A}$R

signaling is likely an integral antitumor pathway for bacterial-ICB cotherapies. Further investigation of the effects of xanthine and hypoxanthine, degradation products of inosine, are warranted.

REFERENCES AND NOTES

1. F. S. Hodi et al., N. Engl. J. Med. **363**, 711–723 (2010).
2. J. R. Brahmer et al., N. Engl. J. Med. **366**, 2455–2465 (2012).
3. R. J. Motzer et al., N. Engl. J. Med. **373**, 1803–1813 (2015).
4. H. Borghaei et al., N. Engl. J. Med. **373**, 1627–1639 (2015).
5. T. N. Gide, J. S. Wilmott, R. A. Scolyer, G. V. Long, Clin. Cancer Res. **24**, 1260–1270 (2018).
6. M. Vétizou et al., Science **350**, 1079–1084 (2015).
7. A. Sivan et al., Science **350**, 1084–1089 (2015).
8. B. Routy et al., Science **359**, 91–97 (2018).
9. V. Matson et al., Science **359**, 104–108 (2018).
10. V. Gopalakrishnan et al., Science **359**, 97–103 (2018).
11. C. M. Dejea et al., Science **359**, 592–597 (2018).
12. J. C. Arthur et al., Science **338**, 120–123 (2012).
13. N. Iida et al., Science **342**, 967–970 (2013).
14. S. Viaud et al., Science **342**, 971–976 (2013).
15. D. T. Le et al., N. Engl. J. Med. **372**, 2509–2520 (2015).
16. S. C. Wei et al., Cell **170**, 1120–1133.e17 (2017).
17. K. A. Ward-Hartstonge, R. A. Kemp, Clin. Transl. Immunology **6**, e154 (2017).
18. R. F. Schwabe, C. Jobin, Nat. Rev. Cancer **13**, 800–812 (2013).
19. G. A. Lugli et al., Appl. Environ. Microbiol. **85**, e03065-18 (2019).
20. D. W. Zheng et al., Nat. Commun. **9**, 1680 (2018).
21. T. Tanoue et al., Nature **565**, 600–605 (2019).
22. F. Wang, Q. Yin, L. Chen, M. M. Davis, Proc. Natl. Acad. Sci. U.S.A. **115**, 157–161 (2018).
23. A. A. Welihinda, M. Kaur, K. Greene, Y. Zhai, E. P. Amento, Cell. Signal. **28**, 552–560 (2016).
24. G. Haskó et al., J. Immunol. **164**, 1013–1019 (2000).
25. B. He et al., J. Exp. Med. **214**, 107–123 (2017).
26. B. Csóka et al., FASEB J. **22**, 3491–3499 (2008).
27. A. Ohta et al., Proc. Natl. Acad. Sci. U.S.A. **103**, 13132–13137 (2006).
28. S. Vigano et al., Front. Immunol. **10**, 925 (2019).
29. C. Cekic, J. Linden, Cancer Res. **74**, 7239–7249 (2014).
30. W. Lasek et al., Acta Pharm. **65**, 171–180 (2015).
31. T. Lioux et al., J. Med. Chem. **59**, 10253–10267 (2016).
32. C. Yao et al., Nat. Commun. **4**, 1685 (2013).
33. B. Samten et al., J. Immunol. **181**, 2056–2064 (2008).
34. B. Samten et al., J. Immunol. **174**, 6357–6363 (2005).
35. B. Jahrsdörfer, G. J. Weiner, Update Cancer Ther. **3**, 27–32 (2008).
36. S. Brugiroux et al., Nat. Microbiol. **2**, 16215 (2016).
37. C. S. Garris et al., Immunity **49**, 1148–1161.e7 (2018).
38. D. Chraa, A. Naim, D. Olive, A. Badou, J. Leukoc. Biol. **105**, 243–255 (2019).
39. M. H. Kucherlapati et al., Gastroenterology **138**, 993–1002.e1 (2010).
40. D. T. Le et al., Science **357**, 409–413 (2017).
41. Y. Shi et al., J. Exp. Med. **217**, e20192282 (2020).
42. K. M. Haigis et al., Nat. Genet. **40**, 600–608 (2008).
43. F. Turroni et al., Appl. Environ. Microbiol. **75**, 1534–1545 (2009).
44. R. D. Pridmore, A. C. Pittet, F. Praplan, C. Cavadini, FEMS Microbiol. Lett. **283**, 210–215 (2008).
45. F. E. Dewhirst et al., Int. J. Syst. Evol. Microbiol. **51**, 1797–1804 (2001).
46. A. E. Frankel et al., Neoplasia **19**, 848–855 (2017).
47. B. A. Helmink, M. A. W. Khan, A. Hermann, V. Gopalakrishnan, J. A. Wargo, Nat. Med. **25**, 377–388 (2019).

SUPPLEMENTARY MATERIALS

science.sciencemag.org/content/369/6510/1481/suppl/DC1
Materials and Methods
Figs. S1 to S22
Tables S1 and S2
References (48–65)
MDAR Reproducibility Checklist

View/request a protocol for this paper from Bio-protocol.

Science

Microbiome-derived inosine modulates response to checkpoint inhibitor immunotherapy

Lukas F. MagerRegula BurkhardNicola PettNoah C. A. CookeKirsty BrownHena RamaySeungil PaikJohn StaggRyan A. GrovesMarco GalloIan A. LewisMarkus B. GeukingKathy D. McCoy

Inosine modulates antitumor immunity

Checkpoint blockade immunotherapy harnesses the immune system to kill cancer cells and has been used with great success to treat certain tumors, but not all cancer patients respond. The efficacy of checkpoint blockade immunotherapy has been shown to depend on the presence of distinct, beneficial bacteria residing in the gut of patients, but how the microbiome mediates such beneficial effects is unclear. Mager *et al.* found that specific bacteria produce a metabolite called inosine that enhances the effect of checkpoint blockade immunotherapy (see the Perspective by Shaikh and Sears). In mouse models, inosine, together with proinflammatory stimuli and immunotherapy, strongly enhanced the antitumor capacities of T cells in multiple tumor types, including colorectal cancer, bladder cancer, and melanoma.

Science, this issue p. 1481; see also p. 1427

View the article online
https://www.science.org/doi/10.1126/science.abc3421
Permissions
https://www.science.org/help/reprints-and-permissions

Use of this article is subject to the Terms of service